Advanced Biomedical Engineering
7: 28–38, 2018.

Original Paper

DOI:10.14326/abe.7.28

R-R Interval Outlier Processing for Heart Rate Variability Analysis using Wearable ECG Devices

Kana EGUCHI,[*,#] Ryosuke AOKI,[*] Suehiro SHIMAUCHI,[**] Kazuhiro YOSHIDA,[*] Tomohiro YAMADA[*]

Abstract Electrocardiograms (ECGs) captured by wearable ECG devices readily contain artifacts due to measurement faults. Since artifacts and R waves have quite similar frequency characteristics, R wave misdetection or R-R interval (RRI) miscalculation may result. Aiming at accurate analysis of heart rate variability (HRV), this paper proposes a new RRI outlier processing method consisting of three steps: evaluating RRI reliability, excluding RRI outlier, and complementing missing RRI. In the first step, the method evaluates the measurement status of all detected R waves and calculates RRI reliability based on the measurement status of a combination of the measurement status of two R waves. Since we target wearable ECG devices used in non-medical environment, the method evaluates R waves based on the threshold electric potential for left ventricular hypertrophy, and determines those exceeding the threshold as artifacts. The method accordingly sets lower reliability to RRIs containing R waves evaluated as artifacts. In the second step, the method excludes all RRIs with low reliability as outliers. These steps may be effective for HRV measures in the time domain, but are not sufficient for analyzing HRV measures in the frequency domain. Resampling the time series RRI data, which is essential for analyzing HRV in the frequency domain, may produce outliers if the target RRIs contain missing values. Our method accordingly complements missing RRIs before data resampling based on RRI characteristics. We postulate that consecutive changes in RRIs follow a simple formula consisting of three components: direct current, low frequency, and high frequency. Our method complements missing values according to the formula, which is calculated from RRIs time series regarded as having been properly measured. To confirm the effectiveness of the method before applying it to ECGs recorded by wearable devices, we evaluated all the steps using pseudo-ECGs generated artificially by adding noise and artifacts to open ECG data. Initial evaluation results showed that the proposed method outperformed conventional method regarding the precision of both time and frequency domain measures of HRV.

Keywords: wearable, electrocardiogram, heart rate variability, measurement fault, outlier processing.

Adv Biomed Eng. **7**: pp. 28–38, 2018.

1. Introduction

A recent study indicates that mental stress may impede healthy balance of the autonomic nervous system (ANS) and trigger mental diseases [1]. ANS activity is related to heart activity, and can be estimated from heart rate variability (HRV), which is derived from the interval between two adjacent R waves (RRI) [2]. To estimate user's ANS activity in daily life by measuring HRV, the device should be easy to use and have minimal effect on user's daily life. Therefore, we focused on shirt-type electrocardiogram (ECG) devices with embedded electrodes and lead wires [3, 4].

While HRV analysis requires accurate RRIs derived from stable ECGs without measurement faults, shirt-type ECG devices readily generate noise and artifacts due to external factors such as body movements, respiration, and perspiration [5], and this causes R wave misdetection or RRI miscalculation. Since HRV features derived from RRI data with miscalculated RRI do not reflect actual heart activity, excluding miscalculated RRI is an essential procedure for both time and frequency domain HRV analysis. Furthermore, while frequency domain measures of HRV require RRI interpolation and data resampling for spectrum analysis, it is difficult to

This study was presented at the Symposium on Biomedical Engineering 2017, Ueda, September, 2017.
Received on July 21, 2017; revised on October 31, 2017; accepted on December 24, 2017.

[*] NTT Service Evolution Laboratories, Nippon Telegraph and Telephone Corporation, Kanagawa, Japan.

[**] NTT Media Intelligence Laboratories, Nippon Telegraph and Telephone Corporation, Tokyo, Japan.

[#] Y-509A, NTT Yokosuka R&D Center, 1–1 Hikari-no-oka, Yokosuka, Kanagawa 239 –0847, Japan.
E-mail: eguchi.kana@lab.ntt.co.jp, kana.eguchi.gh@hco.ntt.co.jp

precisely interpolate RRI time series data with missing values. This may result in miscalculating frequency domain measures of HRV due to interpolation faults such as oscillation of the interpolation function.

In this paper, we propose an RRI outlier processing method consisting of three processes: evaluating RRI measurement status, excluding miscalculated RRIs, and complementing missing RRIs. In the first step, the method discriminates the status of R wave measurements as artifact, noise, or properly measured, and evaluates RRI measurement status in accordance with a combination of the measurement status of two R waves. In addition, the method sets lower reliability to the RRIs containing artifacts and noise in a graded manner. In the second step, the method excludes all RRIs with low reliability, regarding them as outliers. The third step, which only concerns frequency domain HRV analysis, complements missing RRIs according to the trend of properly measured RRIs. This focuses on the fact that frequency domain HRV analysis assumes that RRIs consist of three different frequency components. Changes in RRI trend are based on the frequency characteristics of each component.

2. Related Research

To appropriately understand both the physical and mental conditions of general people in daily life, we focused on HRV analysis using long-term ECG measurement. Wearable ECG devices can be broadly divided into two types: patch-type [6, 7] [**Fig. 1(1)**] and shirt-type [3, 4] [**Fig. 1(2)**]. While the former measures ECG more accurately than the latter, it is difficult for non-medical users to place patch-type devices at appropriate positions for ECG measurements. Since patch-type devices fix measurement electrodes onto the skin through external adapters such as tapes, these external adapters sometimes fail to record appropriate ECG due to slippage of electrodes caused by perspiration. This may disturb the spontaneous daily activities of users. Furthermore, it is difficult for non-medical users to fix measurement electrodes at appropriate positions. Therefore, we focused on the shirt-type devices with embedded electrodes and lead wires, which can be handled easily even by users who have no medical knowledge.

Conventional HRV analysis is performed using four processes (**Fig. 2**): ECG waveform feature extraction, RRI evaluation, HRV feature calculation, and internal status estimation using HRV features such as sleep stages [8] and fatigue [9]. Depending on the service architecture, each process may be implemented separately and only the output data of each process is uploaded for the next process. When using shirt-type ECG devices in daily life, almost all measured ECGs supplied for HRV analysis have not been visually confirmed by medical experts, even though measurement faults may induce noise and artifacts [5]. Therefore, R wave detection and RRI outlier exclusion are quite important to guarantee the accuracy of the calculated HRV features.

Accurate R wave detection methods are broadly divided into two approaches. One is applying filters to the target ECGs [10, 11]. This approach may improve the accuracy of R wave detection without modifying the R wave detection method. The other is to use R wave detection methods that utilize the frequency characteristics of R waves [12, 13]. However, neither approach is able to completely exclude misdetected R waves, which have frequency characteristics similar to those of regular R waves.

Conventional RRI outlier exclusion methods can also be broadly divided into two approaches: one that

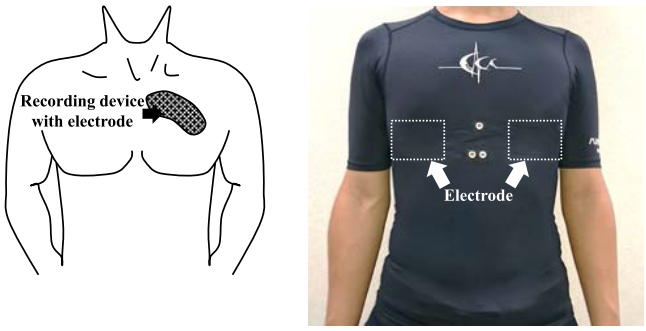

Fig. 1 Examples of wearable ECG devices.

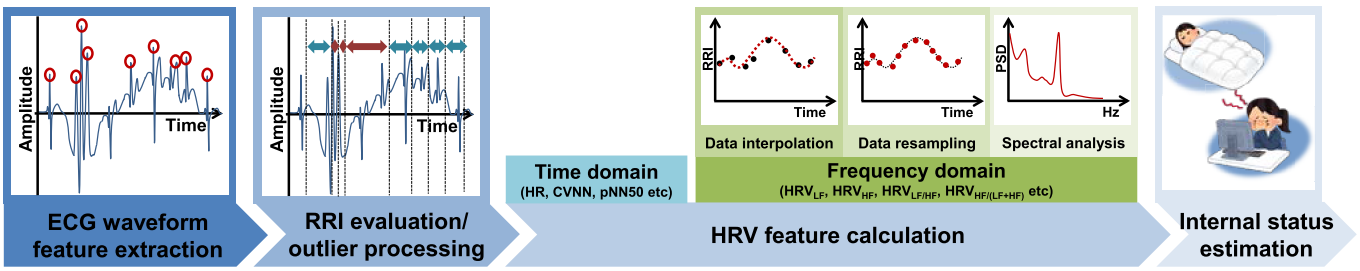

Fig. 2 Processing flow of conventional HRV analysis.

uses the validity of RRI duration and one that uses the measurement status of RRIs. The former approach focuses on either RRI physiological characteristics [12] or RRI change tendencies [14], and excludes RRIs that deviate from assumed rules. However, since both approaches use only time information of RRI, miscalculated RRIs within a reasonable duration are not detected as outliers. The latter approach excludes RRI outliers on the basis of their measurement status [15]. This method focuses on the fact that the electric potential of the QRS complex (hereafter QRS potential), which is the absolute difference between local maxima and local minima of an arbitrary QRS complex (**Fig. 3**), is comparatively stable, as well as the fact that measurement faults usually affect the amplitude of electric potential. Accordingly, it discriminates the measurement status of all detected R waves based on the amplitude as a first step. Since RRI is measured from two adjacent R waves, this method calculates RRI measurement status based on the measurement status of the corresponding R waves, and RRIs with low reliability are excluded as outliers. Combining all the aforementioned RRI outlier exclusion techniques is an effective way to improve the accuracy of time domain measures of HRV (tHRV) [15].

However, unlike time domain HRV analysis, frequency domain HRV analysis requires three preprocessing steps before calculating frequency domain measures of HRV (fHRV): data interpolation, data resampling, and spectral analysis. Since RRIs are unequal spatial data derived from each heart beat, all target RRIs should be equally spaced by data interpolation and data resampling before spectral analysis.

Although interpolation functions such as linear and spline functions do not significantly affect the power spectral density (PSD) used for fHRV calculation [16], missing RRIs give rise to RRI outliers due to oscillation of the interpolation function, especially when using the spline function for interpolation (**Fig. 4**). The fHRV derived from resampled data containing RRI outliers do not appropriately reflect the real heart activity or ANS activity, and may result in misestimation of internal status in the last step of HRV analysis, especially when each process is implemented separately. For this reason, missing RRI sectors should be appropriately processed separately from the conventional data interpolation before fHRV analysis when shirt-type ECG devices are used.

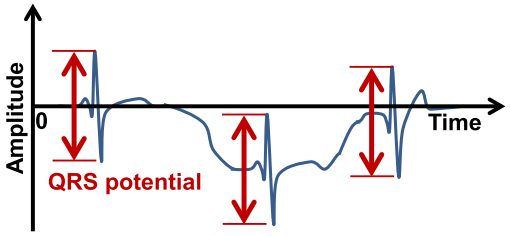

Fig. 3 Schematic diagram of QRS potential.

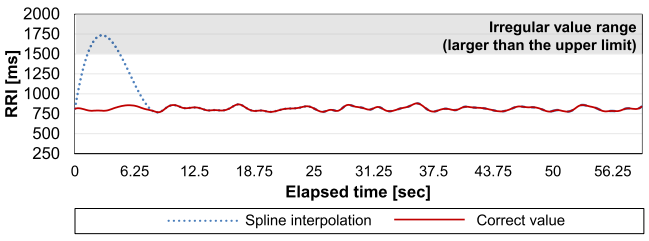

Fig. 4 RRI outliers caused by spline interpolation. Some interpolated RRIs exceed the upper limit of RRI (1500 ms).

3. Proposed Method

To obtain accurate fHRV analysis when using shirt-type ECG devices, we propose a method to complement missing RRI sectors based on the estimated trend of RRI time series data. This method comprises two processes: estimating the trends of properly measured RRIs and using the estimated trends to complement missing RRI sectors. We expect that the accuracy of fHRV feature will be improved by adding our proposed method to the RRI outlier processing method in fHRV analysis, even if the complemented RRIs are not perfectly correct, and this may contribute to improve the estimation accuracy in the last step of HRV analysis. Note that our method assumes in advance that RRI outliers are excluded using the conventional methods [12, 14, 15], and that RRI time series data are divided into two different sectors: a "data sector" consisting of spontaneous RRIs without any missing data, and a "data loss sector" with missing RRIs (**Fig. 5**). Since our method only targets the "data loss sector," we resampled the "data sector" afterwards by conventional interpolation.

3.1 Estimation of RRI trend

This process aims to estimate the data trend in the "data sector" for complementing missing RRIs in the "data loss sector." Since fHRV analysis assumes that in principle

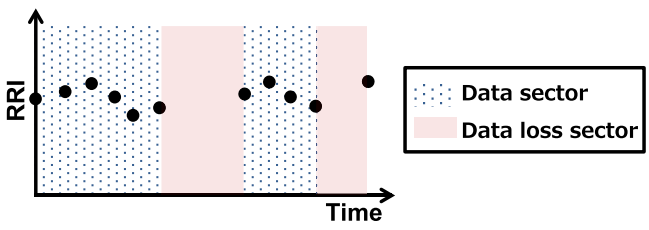

Fig. 5 Schematic diagram of sector classification.

RRIs comprise at least three different components [direct current (RRI_{DC}), low frequency component (RRI_{LF}), and high frequency component (RRI_{HF})] and calculates the cumulative value of each component derived from PSD of target RRIs, our method estimates the major trends of properly measured RRIs based on a simple combination of those three components. This is shown in the following equation [17].

$$estimatedRRI = RRI_{DC} + RRI_{LF} + RRI_{HF} \quad (1)$$

This equation originally assumes that the target frequency of RRI_{LF} ranges from 0.04 to 0.15 Hz, and RRI_{HF} ranges from 0.15 to 0.40 Hz. When shirt-type ECG devices are worn, it is difficult to discriminate measured RRIs derived from physiological changes from artificial fluctuations derived from noise or artifacts, but they are still supposed to contain the global trends of RRI changes. Therefore, we simplify each frequency component using a sine wave that has only one representative frequency, and generate pseudo components of RRI_{DC}, RRI_{LF}, and RRI_{HF} in the missing RRI sector. We approximate the estimated RRI at t seconds in equation (1) to the following equation.

$$\begin{aligned} estimatedRRI = {} & RRI_{DC} \\ & + C_{LF}\sin(2\pi f_{LF}t + \phi_{LF}) \\ & + C_{HF}\sin(2\pi f_{HF}t + \phi_{HF}) \end{aligned} \quad (2)$$

Here, we assume that RRI_{DC} can be estimated by the mean value of properly measured RRIs. Regarding the frequency components, we need to estimate their respective magnitudes (C_{LF} and C_{HF}), representative frequencies (f_{LF} and f_{HF}), and phases (ϕ_{LF} and ϕ_{HF}).

To calculate the representative frequencies f_{LF} and f_{HF}, we employ two different band-pass filters (BPFs) in preprocessing to emphasize the f_{LF} and f_{HF} components separately and identify the peak components as f_{LF} and f_{HF} from the spectra of the respective preprocessed series. In our assumed situation, although some fixed BPFs can be applied, we choose BPFs with frequency characteristics that can be adaptively changed depending on the peak frequencies of RRI_{LF} and RRI_{HF}. We do this to simulate appropriate PSD even when the peak frequencies of f_{LF} and f_{HF} are close to each other. Their characteristics are given based on spectral envelopes of properly measured RRIs at different resolutions, which are obtained by truncating the cepstrum of the RRIs at different orders (**Fig. 6**). The representative frequencies f_{LF} and f_{HF} can be obtained by extracting only one frequency with the highest power aside from DC in the spectrum of each preprocessed RRI series.

The magnitudes of the frequency components, shown as C_{LF} and C_{HF}, are calculated by observing the two BPFs in the time domain. To reflect the amplitude characteristics of the components at f_{LF} or f_{HF}, as well as

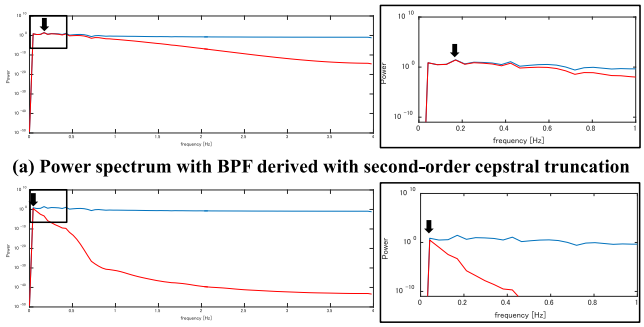

(a) Power spectrum with BPF derived with second-order cepstral truncation

(b) Power spectrum with BPF derived with twentieth-order cepstral truncation

Fig. 6 Power spectra of RRI and estimated frequencies.
Original power spectrum is shown in blue whereas calculated one is shown in red
Peak frequency is annotated with a black arrow
DC component is eliminated by the band-pass filter.

other frequency components in each frequency band, this method calculates local minima and local maxima of the time domain waveform of the BPF output and calculates mean wave heights as the magnitudes C_{LF} and C_{HF}.

In the last step of RRI estimation, this method calculates phase angles of the representative frequencies, shown as ϕ_{LF} and ϕ_{HF} in (2) as follows.

$$\phi_{LF} = \theta_{LF} + \pi/2, \phi_{HF} = \theta_{HF} + \pi/2$$

where $\theta_{LF} = \arctan\dfrac{b(f_{LF})}{a(f_{LF})}$, $\theta_{HF} = \arctan\dfrac{b(f_{HF})}{a(f_{HF})}$ and $a(f_{LF}) + jb(f_{LF})$ and $a(f_{HF}) + jb(f_{HF})$ can be obtained as the complex Fourier coefficients at f_{LF} and f_{HF}.

3.2 Complement of Missing RRI Sectors

After calculations using the aforementioned RRI estimation equation (2), the proposed method complements missing RRI sectors (i.e., "data loss sectors"). Since there is no guarantee that the time interval between the previous RRI and the estimated RRI will become exactly the same as the estimated RRI in a missing RRI sector, and no guarantee that fHRV analysis will be able to discriminate the morphological order of RRIs in principle, this method complements missing RRI sectors at the same resampling rate as the properly measured RRIs in "data sectors." In other words, it interpolates missing RRI sectors in accordance with equation (2) rather than by linear or spline function. Later on, it resamples "data sectors", which consist only of properly measured RRIs, by the conventional interpolation function, and the proceeds to spectral analysis.

4. Experiment

4.1 Outline

To confirm the effectiveness of our method for fHRV analysis when using shirt-type ECG devices, we compared the fHRV calculated from two different RRI outli-

er processing methods; our previously reported outlier exclusion method [15] alone (hereafter conventional method), and the method combining RRI outlier exclusion [15] and missing RRI complement we propose here (hereafter proposed method), to those derived from the reference RRIs. The main purpose of this experiment was to confirm two points: (a) the appropriateness of the complemented values in the missing RRI sector, and (b) the effectiveness of RRI complement in fHRV analysis.

As an initial evaluation of RRI outlier processing in fHRV analysis, we used pseudo-ECG containing noise or artifacts, and compared the calculated values derived from pseudo-ECG with each RRI outlier processing method to those derived from the reference RRIs. Assuming a situation that often occurs in actual HRV analysis when using shirt-type ECG devices, we employed the Pan-Tompkins algorithm (hereafter PTA), which is an R wave detection algorithm that does not appropriately handle noise or artifacts [18], for ECG waveform feature extraction to confirm the effectiveness of different RRI outlier processing methods. The proposed method comprised a function for RRI outlier exclusion based on both time and measurement status [15], and a function for complementing missing RRIs before fHRV analysis. In the experiment we conducted, we first compared resampled RRI tachograms derived from each method, and then checked four kinds of fHRV which frequently used in fHRV analysis: the logarithmic values of HRV_{LF} [$\log(HRV_{LF})$] and HRV_{HF} [$\log(HRV_{HF})$], and the secondary feature values of $HRV_{LF/HF}$ and $HRV_{HF/(LF+HF)}$.

4.2 Experimental conditions

4.2.1 Target data

Among actual ECGs measured by shirt-type wearable ECG devices in daily life, noise and artifacts occur randomly at any time due to measurement faults, and identical noise or artifacts will not be observed repetitively even when the user tries to perform the same movements. Since it is extremely difficult to measure ECGs containing intended noise or artifacts in actual environment, we first evaluated the performance of the proposed method using pseudo-ECGs containing noise or artifacts similar to the actual recorded ECGs.

The main factors affecting the accuracy of R wave detection can be divided into ECG measurement position and severity of noise or artifacts. However, when using the PTA, the effects of noise and artifacts are considered to be greater than from the effects due to different chest leads. Therefore, we evaluated the effects of noise or artifacts by fixing the chest lead.

We used a pseudo-ECG artificially generated by adding noise and artifacts to an open ECG data as the analysis target. When using shirt-type ECG devices, measurement faults mainly resemble or result from a combination of three irregularities defined in the MIT-BIH noise stress test database (NSTDB) [19]. Therefore, we generated the target ECGs by mixing the MIT-BIH arrhythmia database (MITDB) [20] with NSTDB, which regarded as irregular waves such as noise or artifacts, in accordance with the following equation, where n is a real number.

$$targetECG = ECG_{MITDB} + n \times irregWave_{NSTDB} \quad (3)$$

Since NSTDB provides three types of noise or artifacts; baseline wander (BW), electrode motion artifact (EM) and muscle artifact (MA), combining them yields seven patterns. We compared the RRI and fHRV derived from different outlier methods for the seven patterns to those derived from the reference RRIs. Note that the reference RRIs were calculated from R wave annotations distributed in MITDB.

Here we describe the target ECGs we used in this experiment in detail. We employed V5-derived ECGs of ID #100, whose chest lead made it easy to detect R waves in the normal measurement state. The total data length was the first 60 seconds, which was 21,600 samples in MITDB at a sampling rate of 360 Hz. Taking the performance of PTA into consideration, we replaced some ECGs with pseudo-ECGs obtained from equation (3). Since PTA is not effective during and after noise and artifacts [15, 18], the replaced section was set during 30 to 40 seconds of the 60-second segment. This pseudo-ECG was a simulated ECG with the assumption that measurement faults causing noise or artifacts occurred suddenly for 10 seconds (during 30 to 40 seconds of the target data) in daily life, which could be due to body movements or impact on the measurement electrodes. To extract R waves from the original performance of PTA, no preprocessing was used. We synchronized ECG_{MITDB} and $irregWave_{NSTDB}$ with the same sample number and set n in equation (3) as 3. The pseudo-ECG generated is similar to that recorded by wearable ECG devices with dry electrodes (**Fig. 7**). Note that wearable ECG devices with dry electrodes have higher impedance than those with wet electrodes and that our target data assumed minimal noise and artifacts, especially for BW and EM. Thus, our actually measured ECGs were sometimes worse than those of the pseudo-ECGs. We used the data provided as "noise 1" of BW, EM, and MA as $irregWave_{NSTDB}$. When mixing two or more irregular waves, we set the added value of irregular waves as $irregWave_{NSTDB}$. In all, we evaluated the RRI time series derived from seven target ECGs: (i) BW, (ii) EM, (iii) MA, (iv) BW+EM, (v) BW+MA, (vi) EM+MA, and (vii) BW+EM+MA. We compared them with the values of reference RRIs derived from "annotations" of MITDB as

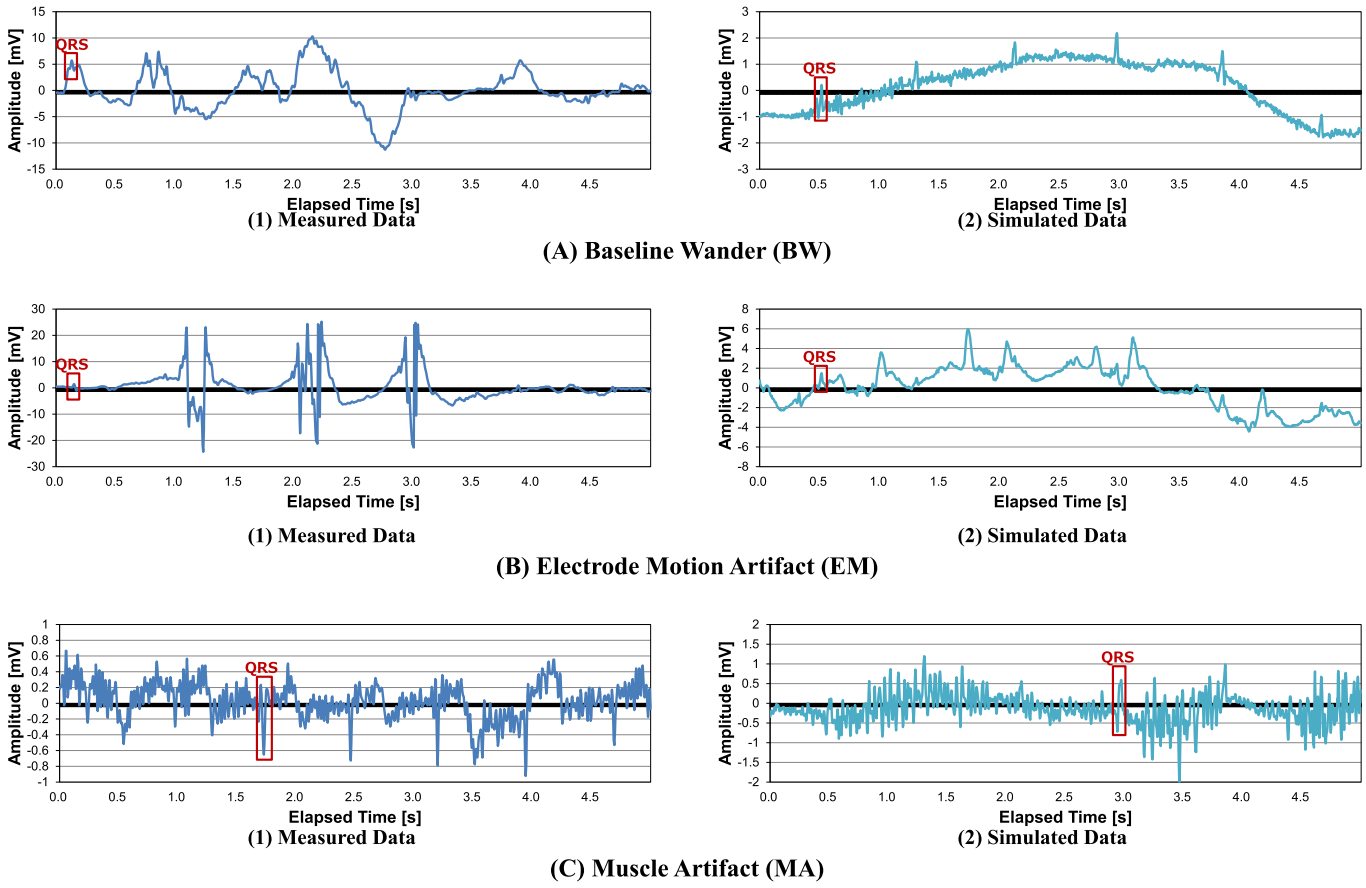

Fig. 7 Comparison of actual ECGs recorded using a wearable device and the simulated ECGs ($n = 3$ in equation 3). QRS complex is annotated by red box. Compared with the amplitude of QRS complex, BW and EM in ECGs recorded using wearable device are worse than the simulated ECGs.

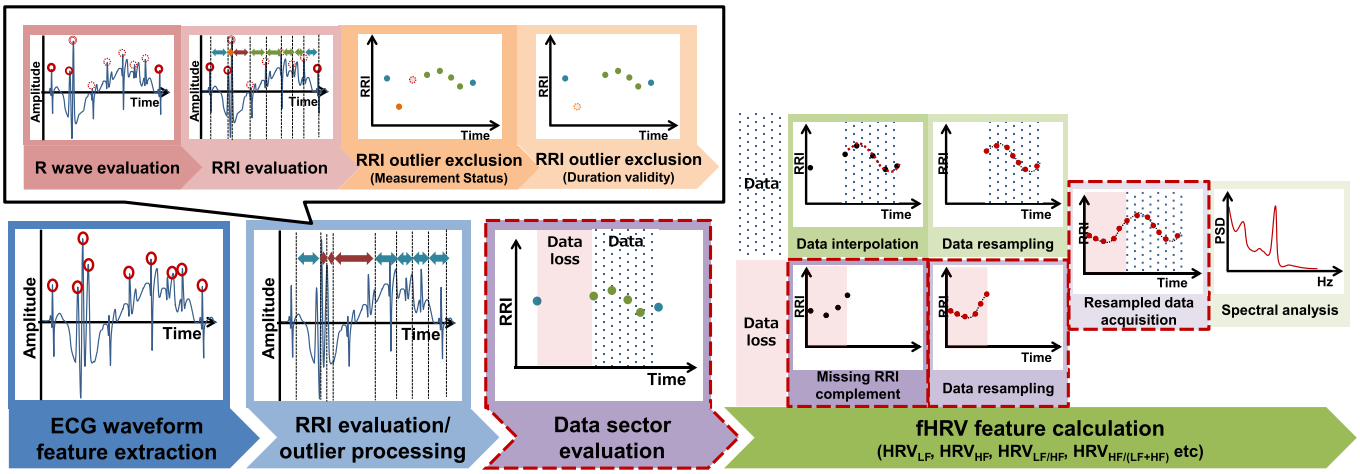

Fig. 8 Processing flow of HRV analysis in the experiment. The processes of the conventional method are highlighted by the black box whereas the processes of the proposed method are highlighted in the black box plus the red dashed boxes.

"Answer."

4.2.2 fHRV analysis conditions

Figure 8 shows the processing flow of fHRV analysis in our experiments. Note that the processes related to the conventional method are highlighted in the bold black box, while the processes of the proposed method are highlighted in the bold black box plus the red dashed

boxes. The details of each process are described in the procedural order in which they occurred.

4.2.2.1. R wave detection algorithm

To confirm the performance of the proposed method with RRI outliers derived from the misdetected R waves due to noise or artifacts, we should employ an R wave detection algorithm that is not stable in those situations. We therefore used PTA, which is widely used as a benchmark R wave detection algorithm [18]. While this algorithm can handle noise and artifacts to some extent, it does not perform well when there is large change of electric potential, and R waves are misdetected during and after noise and artifacts. Consequently, R waves detected as "noise" by PTA are mostly incorrect R waves and not regarded as "properly measured" in HRV analysis.

Moreover, since PTA uses filters and moving average, it cannot calculate electric potential of the maxima of R waves and QRS potential, or acquire the exact observation time of R waves. For this reason, we back calculated the observation time of R waves from the output of PTA. We regarded the maxima within the filter delay of PTA as an R wave and regarded its observation time as that of R wave. We also regarded the minima observed within 0.10 second after an R wave as an S wave, because the maximum duration of the QRS complex among healthy people is 0.10 second [21]. We then regarded the differential value of R and S waves as QRS potential.

4.2.2.2. RRI outlier exclusion

RRI outliers were excluded by combining two methods: one based on the RRI measurement status, and the other based on RRI time validity.

We first excluded RRI outliers based on the measurement status [15]. As a first step of this outlier exclusion method, we evaluated the measurement status of all the detected R waves, which is indispensable for evaluation of RRI measurement status. The QRS potential was calculated from each detected R wave, and the certain R waves with QRS potential above 4.0 mV were regarded as artifacts. This value is the medical threshold for left ventricular hypertrophy, which is a typical cardiovascular disease with high amplitude of QRS potential [21]. Since shirt-type wearable ECG devices are normally used by healthy subjects without any cardiovascular disease, we discarded R waves that exceeded the medical threshold as artifacts. Among those R waves not regarded as artifacts, they were regarded as noise when the differential value between the electric potential of the R wave maxima and the QRS potential amplitude exceeded 1.0 mV. Shirt-type wearable ECG devices normally aim to measure ECGs around chest leads V3 to V4, where the amplitudes of R wave and S wave become approximately the same. However, R waves or S waves are mainly observed when BW occurs, and this is rarely observed when measuring ECGs from the same measurement position. In this case, the difference between the electric potential of the R wave maxima and the QRS potential amplitude deviates from 0 mV. Therefore, we evaluated R waves with the aforementioned threshold of 1.0 mV, which is a quarter of the artifact threshold. R waves that were regarded as neither artifacts nor noise were considered to have been properly measured. The schematic diagram of evaluation of R wave measurement status is shown in **Fig. 9**.

As a second step, we evaluated RRI measurement status based on the R wave measurement status of two adjacent R waves. If one assumes that the R wave measurement status comprises three types (artifact, noise, and properly measured), the combinations of R wave measurement status of two R waves are shown in **Table 1**. Since this method discriminates artifacts and noise

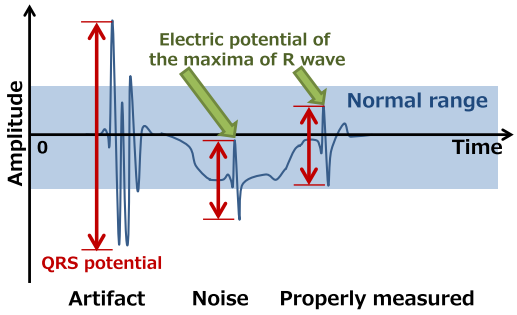

Fig. 9 Schematic diagram of the evaluation of R wave measurement status.

Table 1 Combination of measurement status of two adjacent R waves and reliability of the corresponding RRI. (P: Properly measured R wave, N: Noise, A: Artifact)

#	R waves Combination	Measurement Status	Reliability
1	P P	Both are properly measured R waves	1
2	P N	One properly measured R wave with one noise	0.8
3	N P		
4	N N	Both are noise	0.6
5	P A	One properly measured R wave with one artifact	0.4
6	A P		
7	N A	One noise with one artifact	0.2
8	A N		
9	A A	Both are artifacts	0

on the basis of QRS potential, we define the RRI measurement reliability as shown in **Table 1**, assigning the highest reliability when both were properly measured RRIs and the lowest liability when both are artifacts. We used PTA, which does not appropriately handle noise and artifacts, for R wave detection in this experiment. Consequently, RRIs with measurement reliability less than 1 were excluded as outliers.

After we excluded the RRI outliers based on the measurement status, we evaluated RRI time validity as an RRI outlier exclusion criterion. This method combines two conventional outlier exclusion methods using three sigma rules after extracting RRIs between the upper and lower limits. We set the lower limit to 250 ms and the upper limit to 1,500 ms, using the normal range of healthy subjects as reference [12, 21]. Overall, RRIs that were not excluded by any RRI outlier exclusion method were subject to the next procedure.

4.2.2.3. Missing RRI complement

This step is only employed in the proposed method. We complemented missing RRIs in "data loss sectors," based on the method we described in Section 3. Note that the peak frequency of f_{HF} was extracted from second-order cepstral truncation, whereas the peak frequency of f_{LF} was extracted from twentieth-order cepstral truncation.

4.2.2.4. fHRV analysis

As the first step of fHRV analysis, we generated an RRI tachogram with RRI measurement time on the horizontal axis and measured RRI on the vertical axis. We employed either the spline function or linear function to interpolate the target RRI tachogram at 8-Hz resampling rate. Note that this interpolation step was omitted for the "data loss sectors" in the proposed method, because all data in those sectors were interpolated through the missing RRI complement. In the spectral analysis after data resampling, we set the analysis data window width to 60 seconds, and windowed the data using a Hann window. We calculated PSD using an autoregressive model [17]. We set the order of the autoregressive model to the sixteenth order, where the PSDs at both low and high frequencies become stable regardless of respiratory conditions.

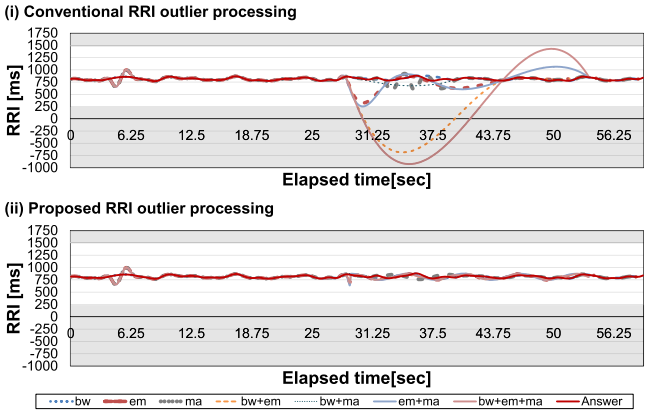

Fig. 10 Comparison of resampled RRI tachograms (cubic spline interpolation).
Shaded values indicate physiologically irregular RRIs in healthy subjects [12].

5. Results

Figure 10 shows the resampled RRI tachograms obtained from analysis with the conventional method and the proposed method, using spline interpolation. Comparing the two, we found that the proposed method prevented oscillation of the interpolation function and all the RRIs were resampled into the applicable RRI range even when the conventional RRI outlier processing caused oscillation. Therefore, the proposed method allowed analysis of RRIs that were excluded from the analysis dataset due to the lack of RRIs in the conventional fHRV analysis.

Figure 11 shows fHRV obtained from different RRI outlier processing methods using spline interpolation, and **Fig. 12** shows the results using linear interpolation. The bars in the right unshaded column are correct values calculated from RRIs derived from R wave annotations of MITDB while the bars in the shaded columns are values calculated from RRIs derived from ECGs with added noise or artifacts and processed by the proposed method (blue bars) or by the conventional method (red shaded bars). These results confirmed that the accuracy of the calculated fHRV was improved by the proposed method, especially for the secondary fHRV such as $HRV_{LF/HF}$ and $HRV_{HF/(LF+HF)}$, regardless of the interpolation function.

6. Discussion

As shown in **Figs. 10 to 12**, the proposed method appropriately complemented missing RRI sectors and improved the precision of all targeted fHRV. These experimental results suggest that a combination of RRI outlier exclusion and missing RRI complement functions is effective for fHRV analysis when shirt-type ECG devices are worn even when using linear interpolation. On the other hand, comparison of the conventional RRI outlier processing method and the proposed method implies that the former, which only uses data interpolation to complement missing RRI sectors, is insufficient for fHRV analysis.

Focusing on **Figs. 11 and 12**, we found that the proposed method substantially improved $HRV_{LF/HF}$ and $HRV_{HF/(LF+HF)}$ for BW+EM and BW+EM+MA regardless of the interpolation function. Furthermore, the accu-

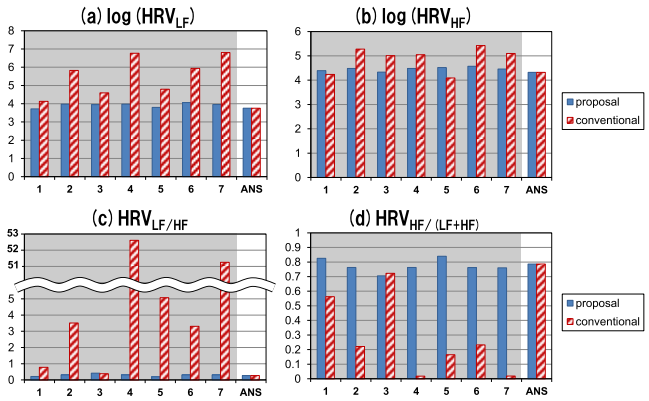

Fig. 11 Comparison of frequency domain measures of HRV when RRIs were analyzed by the proposed outlier processing methods (cubic spline interpolation). (1: BW, 2: EM, 3: MA, 4: BW+EM, 5: BW+MA, 6: EM+MA, 7: BW+EM+MA).

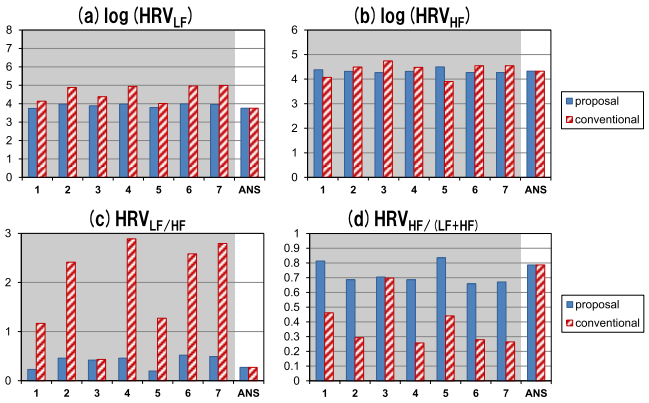

Fig. 12 Comparison of frequency domain measures of HRV when RRIs were analyzed by the proposed outlier processing methods (linear interpolation). (1: BW, 2: EM, 3: MA, 4: BW+EM, 5: BW+MA, 6: EM+MA, 7: BW+EM+MA).

racy of fHRVs derived from analysis using the proposed method was better than using the conventional linear interpolation. This indicates that the proposed complement of missing RRI, which simulates both RRI$_{LF}$ and RRI$_{HF}$, is effective for fHRV analysis. When using the proposed method, cubic spline interpolation, which can smoothly interpolate values, is better than linear interpolation based on comparison with the correct fHRV (ANS in **Figs. 11 and 12**) in these experimental results. Comparing fHRV derived from one irregular wave alone, we found that EM mostly caused miscalculation of fHRV analysis. Since EM causes substantial changes in ECG amplitude, PTA [18] generates misdetected RRIs or rather miscalculated RRIs, which may be applicable for exclusion purposes in RRI outlier exclusion. This may result in oscillation of the interpolation function and derivation of substantially deviated resampled data in the fHRV analysis when using cubic spline function. Although linear interpolation may prevent this oscillation, it does not appear to be sufficient for fHRV analysis. Therefore, this method may be effective for certain data with missing RRIs.

However, the proposed method alone is not very effective in fHRV analysis targeting ECGs with MA alone, where RRI outlier exclusion is not as effective as other methods of handling noise or artifacts [15]. Since the proposed method approximates RRI trends based only on representative frequency, the complemented RRIs deviate from proper RRIs, especially at the end of missing RRI sectors. Since these deviations may degrade fHRV analysis performance, the most appropriate RRI complement function should be identified using various types of RRI data with different types of missing RRIs or RRI trends.

To confirm the feasibility of the proposed method in a practical situation, we conducted a preliminary test with a commercial shirt-type wearable ECG device (Goldwin, C3 fit IN-pulse). In this test, the subject was in a supine resting position with occasional turning over. **Figure 13** shows the target ECG in this evaluation. This ECG contained at least BW and EM due to twisting of the body. In such cases, PTA failed to detect R waves. We calculated secondary fHRVs, HRV$_{LF/HF}$, and HRV$_{HF/(LF+HF)}$ of arbitrary 300-second long RRIs under the same conditions referred to in 4.2.2, apart from the analysis data window width, which was set at 300 seconds for this test. Note that the reference RRIs were measured separately using a wearable Holter ECG device (Suzuken Co. Ltd, Cardy 303 pico+) at the same time, which we visually confirmed that there were no RRI outliers due to measurement faults. **Figure 14(1)** shows the fHRVs derived with different RRI outlier processing methods, using cubic spline interpolation, and **Fig. 14(2)** shows the results using linear interpolation. Both results show that the fHRVs derived from the proposed method are more accurate than those obtained from using the conventional ones even when using linear interpolation. These results indicate that the proposed method is effective in handling long-term time series missing RRIs in fHRV analysis under practical situations.

We used cepstrum analysis to emphasize certain frequency components in the present study, since it is also used for extracting certain data frequencies, such as the respiratory curve from the voltage curve measured by the piezo band [22]. The performance of the proposed method depends on how well the method estimates RRI trend of properly measured RRIs, and hence its validation should be performed using more data. While we estimat-

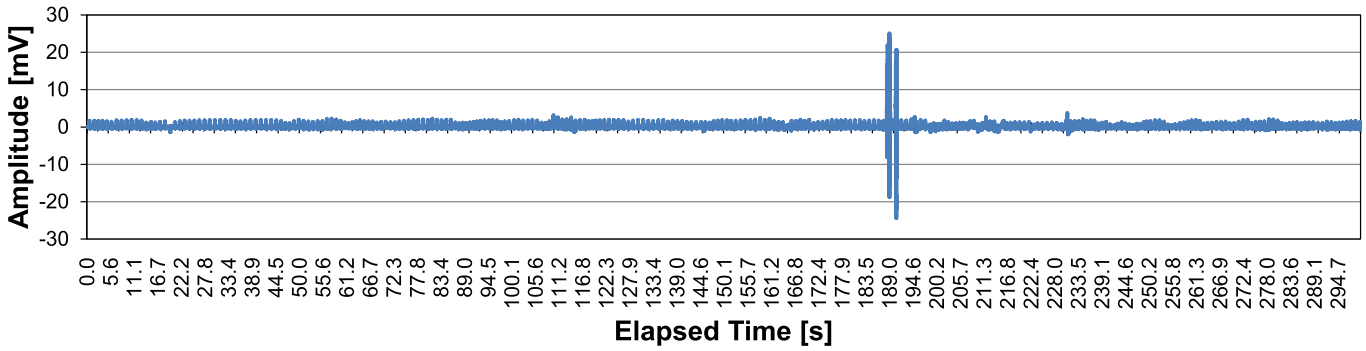

Fig. 13 Target ECG measured by shirt-type wearable ECG device.
EM is observed around 189.0 [s] due to the measurement fault caused by turning over.

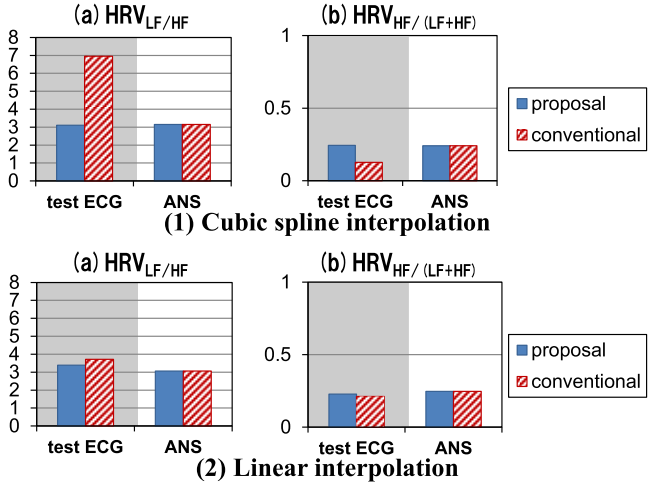

Fig. 14 Comparison of frequency domain measures of HRV between different RRI outlier processing methods.

ed RRI trend from the longest time series of properly measured RRIs in this experiment, we should consider adaptive RRI trend estimation by adjusting the target data length of properly measured RRIs, or optimizing lifter coefficient for further applicable condition when using shirt-type ECG devices in practice.

7. Conclusion

To reduce the effects of noise and artifacts on accurate frequency domain measures of HRV in daily life, we propose an outlier processing method comprising a combination of evaluation of RRI measurement status, exclusion of RRI outliers, and complement of missing RRIs. Since RRI is calculated from two adjacent R waves, the method first discriminates R wave measurement status utilizing the electric potential characteristics of the QRS complex, and on that basis evaluates RRI measurement status. After the method excludes RRIs with lower reliability as outliers, it complements missing RRIs according to the estimated RRI trend derived from properly measured RRI time series data. Experimental results showed that the proposed method improved the accuracy of HRV frequency domain measures as a RRI outlier processing tool for ECGs with noise or artifacts, compared with conventional method. This method potentially contributes to improve the accuracy of various estimation algorithms that use these features.

References

1. Thayer JF, Yamamoto SS, Brosschot JF: The relationship of autonomic imbalance, heart rate variability and cardiovascular disease risk factors. Int J Cardiol. **141**, pp. 122–131, 2010.
2. Task Force of the European Society of Cardiology and the North American Society of Pacing and Electrophysiology: Heart rate variability: standards of measurement, physiological interpretation, and clinical use. Eur Heart J. **17**, pp. 354–381, 1996.
3. Takagahara T, Ono K, Oda N, Teshigawara T: "hitoe" –a wearable sensor developed through cross-industrial collaboration. NTT Technical Review. **12**(9), pp. 1–5, 2014.
4. Shiozawa N, Lee J, Okuno A, Makikawa M: Novel under wear "Smart-Wear" with stretchable and flexible electrodes enables insensible monitoring electrocardiograph. Proc World Engineering Conference and Convention. **2015**, OS7-6-3, pp. 1–2, 2015.
5. Friesen GM, Jannett TC, Jadallah MA, Yates SL, Quint SR, Nagle HT: A comparison of noise sensitivity of nine QRS detection algorithms. IEEE Trans Biomed Eng. **37**(1), pp. 85–98, 1990.
6. Fensli R, Gunnarson E, Gundersen T: A wearable ECG-recording system for continuous arrhythmia monitoring in a wireless tele-home-care situation. Proc IEEE CBMS. **2005**, pp. 407–412, 2005.
7. Lobodzinski SS, Laks MM: New devices for very long-term ECG monitoring. Cardiol J. **19**(2), pp. 210–214, 2012.
8. Takeda T, Mizuno O, Tanaka T: Time-dependent sleep stage transition model based on heart rate variability. Proc IEEE EMBC. **2015**, pp. 2343–2346, 2015.
9. Chiba A, Tsunoda K, Chigira H, Ura T, Mizuno O, Tanaka T: Estimating critical fusion frequency from heart rate variability. IEEE EMBC. **2015**, 2015.
10. Tong DA, Bartels KA, Honeyager KS: Adaptive reduction of motion artifact in the electrocardiogram. Proc Second Joint EMBS/BMES Conf. pp. 1403–1404, 2002.
11. Leski JM, Henzel N: ECG Baseline wander and powerline interference reduction using nonlinear filter bank. Signal Processing.

85, pp. 781–793, 2005.

12. Fujii T, Nakano M, Yamashita K, Konishi T, Izumi S, Kawaguchi H, Yoshimoto M: Noise-Tolerant QRS detection using template matching with short-term autocorrelation. Proc IEEE EMBC. **2013**, pp. 7330–7333, 2013.
13. Shimauchi S, Eguchi K, Takeda T, Aoki R: An analysis method for wearable electrocardiogram measurement based on non-orthogonal complex wavelet expansion. Proc IEEE EMBC. **2017**, pp. 3973–3976, 2017.
14. Yokota Y, Kawamura Y, Matsumaru N, Shirai K: Premonitory symptom of septic shock in heart rate variability. Proc 5th Kuala Lumpur Int'l Conf on Biomedical Engineering. pp. 552–555, 2011.
15. Eguchi K, Aoki R, Yoshida K, Yamada T: Reliability evaluation of R-R interval measurement status for time domain heart rate variability analysis with wearable ECG devices. Proc IEEE EMBC. **2017**, pp. 1307–1311, 2017.
16. Rompelman O: The assessment of fluctuations in heart-rate. *In*: Kitney RI, Rompelman O eds. The Study of Heart-rate Variability. Oxford, Clarendon Press, pp. 59–77, 1980.
17. Inoue H: Cardiovascular Diseases and Autonomic Nervous Function, Second Edition. Igaku-Shoin, 2001 (in Japanese).
18. Pan J, Tompkins WJ: A real-time QRS detection algorithm. IEEE Trans Biomed Eng. **32**(3), pp. 230–236, 1985.
19. Physionet, The MIT-BIH Noise Stress Test Database, http://physionet.org/physiobank/database/nstdb/
20. Physionet, The MIT-BIH Arrhythmia Database, http://physionet.org/physiobank/database/mitdb/
21. University of Utah, ECG Learning Center, http://ecg.utah.edu/
22. Ota K, Ishikawa Y, Tanaka M, Joe K: A stress indexing method by respiratory variability analysis. IPSJ SIG Technical Report. **2015-MPS-103/2015-BIO-42**(22), pp. 1–6, 2015 (in Japanese).

Kana Eguchi

Kana Eguchi received the M.S. degree in informatics in 2012 from Kyoto University, Japan. She joined Nippon Telegraph and Telephone Corporation (NTT) in 2012, and has been engaged in research on network middleware and medical engineering at NTT Service Evolution Laboratories. Her current research interest includes Biosignal processing, Wearable/Ubiquitous Computing, and Medical Engineering. She is a member of the Institute of Electronics, Information, and Communication Engineers (IEICE), the IEEE Engineering in Medicine and Biology Society, and Japanese Society for Medical and Biological Engineering (JSMBE).

Ryosuke Aoki

Ryosuke Aoki received M.S. and Ph.D. degrees in information Sciences from Tohoku University in 2007 and 2014, respectively. He joined Nippon Telegraph and Telephone Corporation (NTT) in 2007, and is currently working in NTT Service Evolutions Laboratories. His current research interests include Human Computer Interaction, Medical Engineering and Wearable/Ubiquitous Computing. He is a member of the Information Processing Society of Japan (IPSJ).

Suehiro Shimauchi

Suehiro Shimauchi received B.E., M.E., and Ph.D. degrees from Tokyo Institute of Technology in 1991, 1993, and 2007, respectively. Since joining Nippon Telegraph and Telephone Corporation (NTT) in 1993, he has been engaged in research on Acoustic signal processing and Biosignal processing. He is now a senior research engineer at NTT Media Intelligence Laboratories. He is a member of IEEE, the Institute of Electronics, Information, and Communication Engineers (IEICE), and the Acoustical Society of Japan (ASJ).

Kazuhiro Yoshida

Kazuhiro Yoshida received the B.S. and M.S. degrees in Engineering from Tokyo Institute of Technology in 1994 and 1996, respectively. He joined Nippon Telegraph and Telephone Corporation (NTT) in 1996. He currently works on research and development of sensing technology and its application at NTT Service Evolution Laboratories.

Tomohiro Yamada

Tomohiro Yamada is a Project manager & Executive Research Engineer, Supervisor, Networked Robot and Gadget Project, NTT Service Evolution Laboratories. He received the M.S. in electronics engineering from Niigata University in 1992 and the MBA from the University of Birmingham, UK, in 2007. He joined NTT in 1992, where he has been engaged in research on Content distribution systems and Technologies to support the Human-Robot communication. He is Director of i-RooBO Network Forum Institute, Vice Chair of IEICE Technical Committee on Life Intelligence and Office Information Systems, and also a member of the Association for Computing Machinery (ACM), the Institute of Electrical and Electronics Engineers (IEEE), and the Information Processing Society of Japan (IPSJ).